# BISTATIC SCATTERING CHARACTERISTICS OF A WIND PARK TURBINE DERIVED FROM AN UAV-MOUNTED RECEIVER RECORDING C-BAND WEATHER RADAR SIGNALS

E. Colak, B.V. Patel, A. Vyas, R. Zichner, M. Chandra

Chemnitz University of Technology, Faculty of Electrical Engineering and Information Technology,

Professorship of Microwave Engineering, 09107 Chemnitz, Germany –

(emre.colak, bhavinkumar-vishnubhai.patel, aastha.vyas, ralf.zichner, madhu.chandra)@etit.tu-chemnitz.de

**KEY WORDS:** Weather Radar, Wind Turbine Interference, Wind Turbine Clutter, Bistatic Radar Scattering, Unmanned Aearial Vehicle (UAV)

**ABSTRACT:**

As a result of increasing use of wind energy as a sustainable source of electricity, large Wind Parks with numerous Wind Turbines have been constructed. Wind turbines are extremely tall objects consisting of stationary and moving parts. The presence of wind turbines in the vicinity of weather radar systems can significantly impact their performance, leading to false alarms and errors in radar measurements. Accurate weather forecasting is challenging in this circumstance. Large Radar Cross Section (RCS) of wind turbines results in interference, also known as Wind Turbine Clutter (WTC) or Wind Turbine Interference (WTI), within and beyond the radar main beam, Multipath Interference (MPI), and phenomena referred to as ”shadowing effects” behind the wind turbines. These effects vary significantly in both time and space as a result of various wind turbine operations and meteorological conditions. It can often be difficult to distinguish wind turbine returns from weather-like signals. For the assessment of WTC or WTI, it is essential to understand the scattering properties of these wind turbines. In this paper, the bistatic scattering characteristics of a wind park turbine using a Unmanned Aerial Vehicle (UAV)-mounted receiver recording C-band weather radar signals were investigated by determining the average received power ($P_{Rx_{Avg}}(\theta_s)$) and RCS of wind turbine as a function of the scattering angle. For this purpose, the measurements and data provided by the German Meteorological Service (DWD, Deutscher Wetterdienst) were utilised. The average received power as a function of scattering angle ($\theta_s$) was calculated by using I-Q (In-phase and Quadrature) signals. Forward, back and side scattering of the calculated average received power were analysed separately. Moreover, Front-to-Back ratio, Front-to-Right side ratio and Front-to-Left side ratio were calculated and compared using forward, back and side scatter values. RCS values were also calculated depending on the scattering angle ($\theta_s$) of the wind turbine.

## 1. INTRODUCTION

As the world’s energy needs have increased in recent years, wind energy has become an important tool as one of the sustainable and renewable energy sources. The global installed capacity of wind power increased from 60.8 GW to 93 GW worldwide in 2020 and continues to increase year on year (Elgendi et al., 2023). Especially in Germany during the past few decades, both onshore and offshore wind energy have increased their gross electricity production. Wind energy, which is seen as the most important renewable energy source in Germany, is expected to support the country’s entire energy system as it moves away from fossil fuels. There were 28443 onshore wind turbines (WT) in Germany as of the end of 2022 (Hegler and Plettemeier, 2019), (BWE, 2022), (Wehrmann, 2023).

WTs are extraordinarily tall structures with both stationary and moving components. The effectiveness of weather radar systems can be considerably impacted by the presence of wind turbines nearby, resulting in false alarms and inaccurate radar observations. WT produce clutter from contributions inside and outside the radar main beam, multi-path effects, as well as what are known as ”shadowing” effects behind the WT, due to their large Radar Cross Section (RCS) (Böhme and Seltmann, 2017), (Patel et al., 2023), (Chandra and Gekat, 2018), (Norin and Haase, 2012).

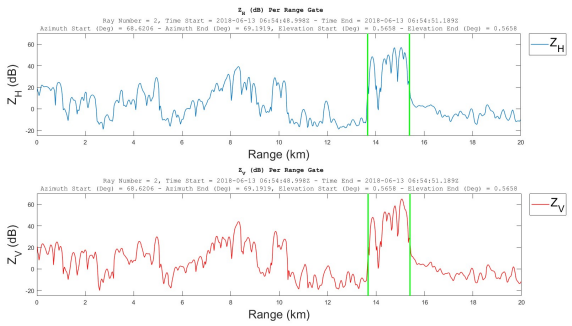


**Figure 1.** Reflectivity in ”H” and ”V” polarisations over a WPA.

In this study, WT detections within the radar’s main-beam line of sight were referred to as Wind Turbine Clutter (WTC), whereas detection of the multi-path effect over the WT’s region was referred to as Multipath Interference (MPI), and the so-called ”shadowing” effect caused by the radar main-beam and its side-lobes was referred to as Wind Turbine Interference (WTI).

Figure 1 shows an example of a reflectivity measurement over a densely spaced WT area, called Wind Park Area (WPA). This measurement was made directly over the WPA at a fixed azimuth and elevation. The green bars in the figure represent the

WPA (13.8 - 15.5 km). As can be seen, reflectivity values of a Wind Park are in the region of 20 – 60 dBs due to the WTC. These values are comparable to the behaviour of moderate to very severe rain conditions.

Understanding the scattering characteristics of these wind turbines is crucial for the evaluation of WTC, WTI, and/or MPI. In this context, the average received power ($P_{avg}$) and RCS of a WT were calculated as functions of the scattering angle ($\theta_s$) in order to explore the bistatic scattering characteristics of a wind park turbine using an Unmanned Aerial Vehicle (UAV)-mounted receiver recording C-band weather radar signals. The German Meteorological Service's (DWD, Deutscher Wetterdienst) measurements and data were used for this purpose. Furthermore, forward, back and side scattering of the calculated $P_{avg}$ were analysed separately. Using forward, back and side scatter values Front-to-Back ratio, Front-to- Right side ratio and Front-to-Left side ratio were calculated and compared.

## 2. STUDY AREA AND DATA USED

A WT with a nacelle height of 135 m and rotor blades of 101 m was used in the measurement. The WT was located on a WPA in Hannover, Germany (Figure 2).


**Figure 2.** WT's location and UAV flight path.

The weather radar was about 23 km from the WT. The line of sight of the main radar beam is shown in red, while the flight path of the UAV is shown in green (Figure 2).

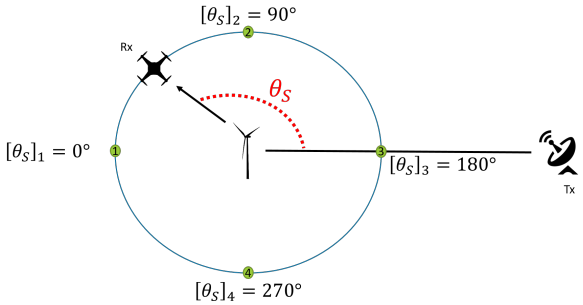


**Figure 3.** Bistatic scattering geometry.

The scattering geometry of the UAV measurement as a Bistatic radar measurement can be seen in Figure 3. Here, position 1 ($\theta_S = 0°$) of the UAV is forward scattering, while position 3 ($\theta_S = 180°$) is backscattering. 2 ($\theta_S = 90°$) and 4 ($\theta_S = 270°$) are the positions of side scattering.

In total, 11 different flights were conducted (Table 1).

| Flight Time [h:min] | Polari -sation | Flight Path/ Position | Radius [m] | Altitude [m] |
|---|---|---|---|---|
| 09:22 | H | 180° | 300 | different heights |
| 09:47 | H | 180° | 300 | different heights |
| 11:00 | H | circle around | 200 | 50 |
| 11:49 | H | half circle | 200 | 75 |
| 12:08 | H | half circle | 200 | 75 |
| 12:23 | V | circle around | 200 | 75 |
| 12:37 | V | circle around | 200 | 50 |
| 15:03 | H | 90° | 200 | 75 |
| 15:26 | H | 0° | 250 | different heights |
| 15:48 | H | 0° | 1000 | different heights |
| 15:54 | H | 0° | 1000 | different heights |

**Table 1.** UAV flight information.

DWD's C-Band HNR (Hannover) radar (*Tx*) was used in the measurement campaign. The radar was directly pointing to the specific WT (fixed radar beam) with a selected PRF and pulse lengths. During the flight the receiver antenna on the UAV (*Rx*) was pointed steadily to the WT. The UAV has a C-Band receiver and matched-filter to detect the pulses. Sampling rate of the UAV is 160 *MHz*, and the antenna gain is 4 *dBi*. There were 1600 samples of I and Q (In-phase and Quadrature) data per pulse in total.

Within the context of this study, the analysis focuses on the outcomes derived from the flight conducted specifically at 11:00.

## 3. METHODOLOGY

A bistatic measurement setup was used to measure the scattering behaviour of a WT (Figure 3). In this context, the $P_{avg}$ on the UAV and the RCS of the WT were measured.

The received complex signal ($S_{pq}$) as a function of scattering angle ($\theta_s$) at the Rx antenna represented mathematically as (Eq. 1).

$$S_{pq}(\theta_s) = I_{pq} + jQ_{pq} \tag{1}$$

Where $I$ and $Q$ are the In-phase and Quadrature components. The variable $q$ represents the transmit polarisation state, while $p$ represents the receive polarisation state. Based on this complex signal the average received power $P_{avg}$ of time series can be calculated as (Eq. 2).

$$[P_{pq}(\theta_s)]_{avg} = \langle |S_{pq}|^2 \rangle = \frac{1}{M} \sum_{n=1}^{M} (S_{pq}^n)^* S_{pq}^n \tag{2}$$

Where $M$ denotes the total number of pulses within the temporal mean, $S_{pq}$ symbolizes the original time series, while the "$*$" denotes the operation of complex conjugation.

In bistatic radar systems, a notable distinction arises as the transmit ($Tx$) and receive ($Rx$) antennas are physically separate and positioned at considerable distances from each other. The bistatic radar cross-section of a specific target is influenced by multiple factors encompassing its geometrical configuration, size, shape, and material characteristic, as well as the polarisation and frequency of the incident radiation. Notably, the bistatic RCS exhibits distinguishable characteristics when compared to the monostatic RCS. This disparity arises due to the substantial impact of the relative orientations of the transmitter, target, and receiver on the RCS values (Bredemeyer et al., 2018), (Bredemeyer et al., 2019).

The radar equation of a point target in bistatic form is mathematically given as follows (Eq. 3) (Richards et al., 2010).

$$P_{Rx}(\theta_s) = \frac{P_{Tx} \cdot G_{Tx}}{4\pi R_1^2} \cdot \sigma \cdot \frac{1}{4\pi R_2^2} \cdot A_e \tag{3}$$

Where $\frac{P_{Tx} \cdot G_{Tx}}{4\pi R_1^2} \left[\frac{W}{m^2}\right]$ is the power density of the radiating antenna to the WT. Here, $P_{Tx}$ $[W]$ is the transmitted power, $G_{Tx}$ is the transmitter gain, and $R_1$ $[m]$ is the distance from weather radar ($Tx$) to the WT. $\sigma$ $\left[m^2\right]$ is the RCS. $\frac{1}{4\pi R_2^2}$ is the re-radiated power from the WT to the UAV-antenna ($Rx$). Here, $R_2$ $[m]$ is the distance from WT to $Rx$. $A_e$ is the effective antenna aperture of $Rx$-antenna. $A_e$ is mathematically defined as follows (Eq. 4).

$$A_e = \frac{G_{Rx} \cdot \lambda^2}{4\pi} \tag{4}$$

Where $G_{Rx}$ is the received gain, and $\lambda$ $[m]$ is the wavelength.

By utilising Eq. (3) and (4), these equations for RCS ($\sigma$) can be solved. Then RCS ($\sigma$) can be expressed as follows (Eq. 5).

$$\sigma(\theta_s) = \frac{P_{Rx}(\theta_s) \cdot (4\pi)^3 \cdot R_1^2 \cdot R_2^2}{P_{Tx} \cdot G_{Tx} \cdot G_{Rx} \cdot \lambda^2} \tag{5}$$

## 4. RESULTS AND DISCUSSION

Firstly, the average power ($[P_{Rx}(\theta_s)]_{avg}$) is calculated for each scattering angle (Figure 4).

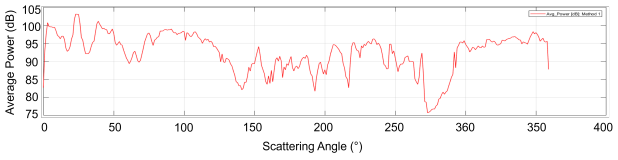


**Figure 4.** Average power over scattering angle.

The received average power for the UAV is between 90 and 95 dB. Notably, the maximum power received occurs at an angle of 23°, measuring 103.6 dB, while the minimum power received transpires at 273°, measuring 75.72 dB. As seen in the figure, direct received power is more pronounced with less backscattering echoes in the remaining area, whereas backscattering echoes are more common in the scattering angle range of 140°to 290°. As seen in the Figure 4, a significant decline in the average power per scattering angle is evident at the 273° angle. This decline is attributed to a simultaneous decrease in incident power coupled with an increased occurrence of backscattering, ultimately leading to a lower average power per scattering angle.

The results of Figure 4 are detailed in Table 2.

| **Power [dB]** | |
|---|---|
| Max. Power | 103.6 |
| Min. Power | 75.72 |
| Avg. Power Range | 90-95 |
| At 0° | 83.07 |
| At 180° | 88.69 |
| At 90° | 98.71 |
| At 270° | 86.72 |

**Table 2.** Comparison of received power values.

Figure 5 and 6 provides more detailed plots depicting the forward- ($\theta_S = 0°$), back- ($\theta_S = 180°$), and side-scatterings ($\theta_S = 90°$and $\theta_S = 270°$), respectively, offering a comprehensive visual representation of these scattering phenomena.

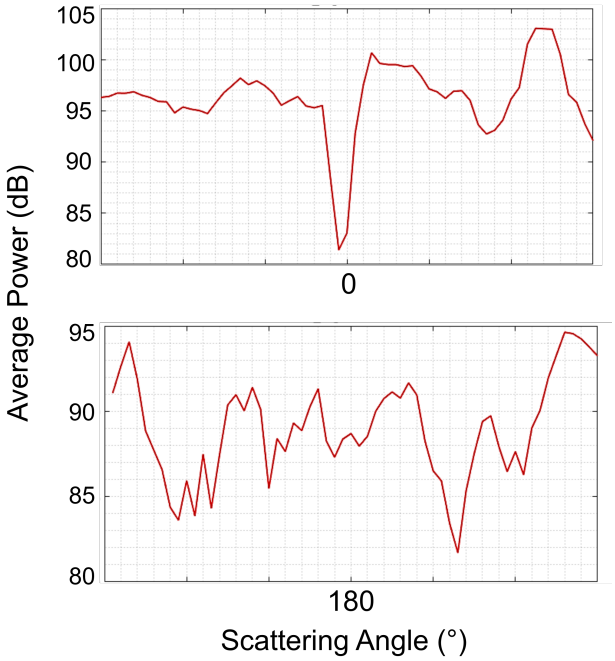


**Figure 5.** Forward- ($\theta_S = 0°$) and back-scattering ($\theta_S = 180°$).

A notable observation is that the power range varies for all types of scattering, thereby providing insights into the received power within the respective areas. In Figure 5, the plot for the Forward scattering ($\theta_S = 0°$), wherein the average power exceeds 95 dB. Notably, there is a significant drop in power at the 0°/360°position, indicating that the UAV is positioned directly behind the WT. This alignment reduces the power reception due to obstructed line-of-sight.

The plot for backscattering ($\theta_S = 180°$), as depicted, showcases the UAV positioned in front and facing the WT. The fluctuating

values indicate a higher presence of reflected signals from the WT, resulting in a lower overall power for the backscattering, which remains below 95 dB.

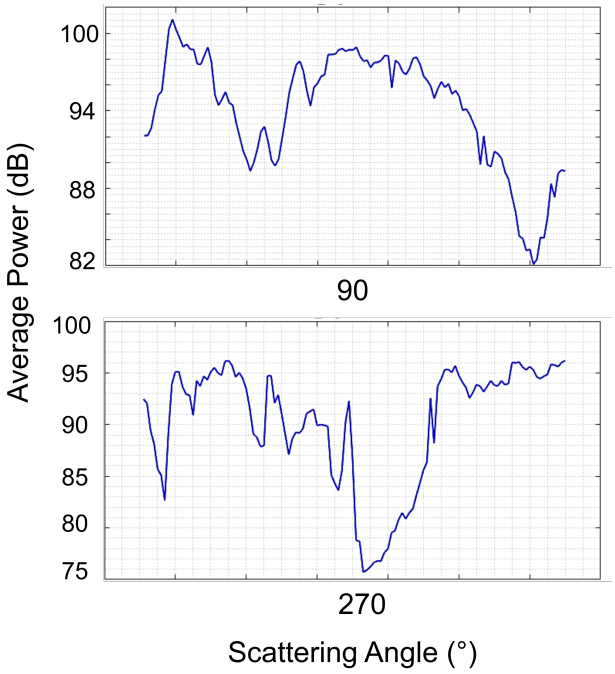


**Figure 6.** Right-side- ($\theta_S = 90°$) and left-side-scattering ($\theta_S = 270°$).

The plot for Right-side scattering ($\theta_S = 90°$) represents the reception when the UAV is positioned next to the right side of a WT (Figure 6). Notably, the average power experiences a drop at 142°, which can be attributed to an increase in backscattering as the UAV approaches the front end of the WT.

The plot for Left-side scattering ($\theta_S = 270°$) represents the reception when the UAV is navigating along the left side of the WT (Figure 6). Notably, due to the prevalence of backscattering being greater than that of the incident radar signal, the average power experiences a drop to 75.72 dB precisely at 173°.

Consequently, as the backscatter from the WT diminishes, there is a decline in power around 170°, followed by a gradual increase (Figure 5). As a results, the average power demonstrates a decrease as the ratio of backscattering to incident signal intensifies.

The Table 3 shows the power ratios according to the location of the UAV.

| | |
|---|---|
| **Front-to-back ratio** | 0.94 |
| **Front-to-right side ratio** | 0.84 |
| **Front-to-left side ratio** | 0.96 |

**Table 3.** Power ratios.

The Figure 7 presents plots depicting the average power (dB) over 1600 samples at the scattering angles ($\theta_s$) of 0°, 90°, 180°, and 270°, respectively.

The Figure 7 provides observations regarding the variation of average peak power across the displayed scattering angles. Specifically, at 0°, the average peak power is observed to be approximately 116 dB, which subsequently increases to approximately 122 dB at 90°.

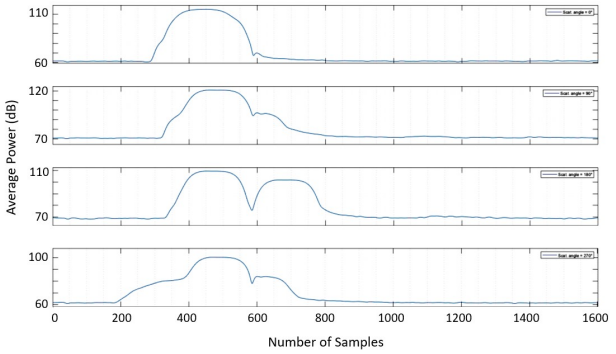


**Figure 7.** Average power (dB) over 1600 samples at the scattering angles ($\theta_s$) of 0°, 90°, 180°, and 270°, respectively.

However, there is a drop in the average peak power to 110 dB at 180°and further decreases to around 100 dB at 270°. Additionally, it is noticeable that the overall signal power undergoes changes across the scattering angles, with values of 62 dB, 70 dB, 68 dB, and 62 dB at 0°, 90°, 180°, and 270°, respectively. The peak observed around 400 samples corresponds to the incident power originating from the weather radar, while the other peaks are likely attributed to the backscattering effects resulting from the wind turbine.

As the UAV moves in front of the wind turbine, specifically within the scattering angle range of 90°to 270°, there is a noticeable decline in the average power of the signal. This reduction can be attributed to an increase in backscattering from the wind turbine, as observed in Figure 5 and 6.

Consequently, this higher level of backscattering contributes to the lower average power per scattering angle in this region.

Figure 8 shows the calculated RCS values of the WT.

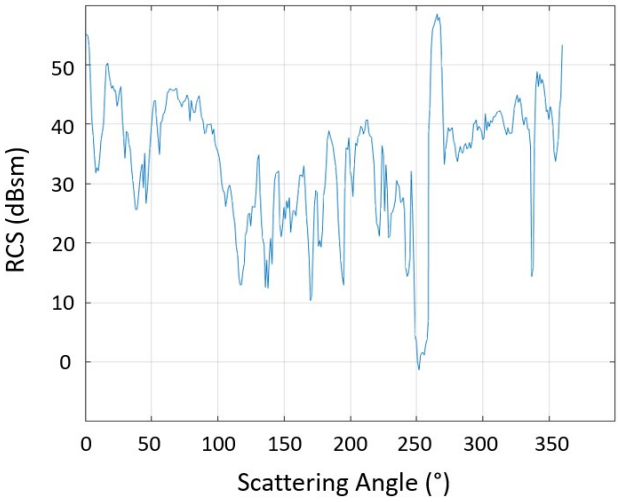


**Figure 8.** RCS (dBsm) values of the WT over the scattering angle (°).

The RCS of a wind turbine serves as a measurement reflecting the radar signal it emits. The RCS is subject to variation depending on the scattering angle, which denotes the angle between

the incoming radar signal and the direction of the scattered signal. In the context of bistatic radar systems, the scattering angle deviates from the incoming radar signal angle due to the disparate locations of the radar transmitter and receiver.

By considering the RCS in relation to the scattering angle characteristics of the wind turbine, bistatic radar systems can optimize the placement of both the transmitter and receiver, as well as design the radar signal to mitigate the influence of scattering effects.

A high RCS value observed at a specific scattering angle indicates that the wind turbine exhibits strong reflectivity towards the incoming radar signal at that particular angle, resulting in a more pronounced signal return. Conversely, a low RCS value at other scattering angles signifies reduced reflectivity of the wind turbine, resulting in a weaker signal return.

Figure 8 illustrates the relationship between the RCS values (in dBsm) and the scattering angles for the wind turbine. A higher dBsm value corresponds to a larger RCS, indicating a more reflective wind turbine. Consequently, a wind turbine with a significant RCS will yield a stronger radar signal, rendering it more detectable and trackable by a radar system.

Based on the provided plot, it can be deduced that the wind turbine exhibits a relatively larger RCS at a scattering angle of approximately 265°compared to other scattering angles. Conversely, at a scattering angle of around 250°, the wind turbine displays a smaller RCS.

## 5. CONCLUSION

In recent years, there has been a discernible upward trajectory in the adoption of wind energy in Europe, particularly in Germany. However, the escalating number of wind turbines has given rise to challenges in weather radar measurements, leading to compromised accuracy in weather forecasts. The presence of wind turbines introduces interferences, such as WTC, MPI, and WTI, owing to their significant RCS values. Consequently, a comprehensive understanding of the scattering characteristics exhibited by these wind turbines assumes utmost importance in evaluating and addressing the mitigation of WTC, WTI, and/or MPI. Accordingly, the primary objective of this study was to ascertain these scattering properties, thereby facilitating a systematic assessment of WTC, WTI, and/or MPI.

For this purpose, received average power ($P_{Rx_{Avg}}(\theta_s)$), power ratios (Front-to-back ratio, Front-to-right side ratio, and Front-to-left side ratio) according to the location of UAV, and RCS values were calculated.

An intriguing observation is the variation in power range across all types of scattering, which offers valuable insights into the magnitude of received power within the corresponding regions. The average received power recorded by the UAV falls within the range of 90 to 95 dB. It is worth noting that the highest power reception is observed at an angle of 23°, reaching a magnitude of 103.6 dB, whereas the lowest power reception occurs at 273°, measuring 75.72 dB.

Based on the RCS calculations, it can be inferred that the wind turbine demonstrates a comparatively higher Radar Cross Section (RCS) at a scattering angle of approximately 265°when compared to other scattering angles. Conversely, at a scattering angle of around 250°, the wind turbine exhibits a smaller RCS value.

As part of future investigations, it is recommended to conduct similar measurements under precipitation conditions and take into account the rotational status of wind turbine rotors. This would provide valuable insights into the potential impact of these factors on the scattering characteristics of wind turbines. By considering these additional variables, a more comprehensive understanding of the scattering behavior can be obtained, leading to enhanced accuracy and applicability of the findings.

## ACKNOWLEDGEMENTS

We would like to thank Mr. Shivang Chandreshbhai Bhayani and Mr. Rohullah Nikzad, master students enrolled in the Information and Communication Systems programme at Chemnitz University of Technology, for their contribution to this work. We would also like to thank the German Meteorological Service (DWD, Deutscher Wetterdienst) for sharing the data utilized in this study.

## REFERENCES

Böhme, T., Seltmann, J. E., 2017. Wind turbine issues in germany. *38th Conference on Radar Meteorology*, AMS.

Bredemeyer, J., Schrader, T., Sandmann, S., 2018. Measurements for classification of single wind turbine echoes. *2018 19th International Radar Symposium (IRS)*, IEEE, 1–10.

Bredemeyer, J., Schubert, K., Werner, J., Schrader, T., Mihalachi, M., 2019. Comparison of principles for measuring the reflectivity values from wind turbines. *2019 20th International Radar Symposium (IRS)*, IEEE, 1–10.

BWE, 2022. German wind energy in numbers. https://www.wind-energie.de/english/statistics/statistics-germany/ (31 December 2022).

Chandra, M., Gekat, F., 2018. Interference in weather radars caused by windparks: Scattering model for weather radar signal processing. *12th European Conference on Antennas and Propagation (EuCAP 2018)*, IET, 1–4.

Elgendi, M., AlMallahi, M., Abdelkhalig, A., Selim, M. Y., 2023. A review of wind turbines in complex terrain. *International Journal of Thermofluids*, 100289.

Hegler, S., Plettemeier, D., 2019. Simulative investigation of the radar cross section of wind turbines. *Applied Sciences*, 9(19), 4024.

Norin, L., Haase, G., 2012. *Doppler weather radars and wind turbines*. INTECH Open Access Publisher.

Patel, B. V., Colak, E., Vyas, A., Chandra, M., Zichner, R., 2023. Processing of weather radar raw IQ-data towards the identification and correction of wind turbine interference–Project RIWER: Removing the Influence of Wind Park Echoes in Weather Radar Measurements. *Advances in Radio Science*, 20, 67–76.

Richards, M. A., Scheer, J., Holm, W. A., Melvin, W. L., 2010. *Principles of modern radar*. SciTech Publishing.

Wehrmann, B., 2023. German onshore wind power – output, business and perspectives. https://www.cleanenergywire.org/factsheets/german-onshore-wind-power-output-business-and-perspectives (13 February 2023).